Korean J. Chem. Eng., **30**(4), 871-877 (2013)
DOI: 10.1007/s11814-012-0190-1

H_2S oxidation by multi-wall carbon nanotubes decorated with tungsten sulfide

Ali Mohamadalizadeh*,†, Jafar Towfighi, Morteza Adinehnia*, and Hamid Reza Bozorgzadeh***

*Gas Research Division, Research Institute of Petroleum Industry, West Boulevard,
Azadi Sport Complex, Tehran 14665-1998, Iran
**Department of Chemical Engineering, Tarbiat Modares University, Aleahmad Highway, Tehran 14115-143, Iran
(*Received 23 November 2011 • accepted 5 November 2012*)

Abstract−Tungsten sulfide catalysts decorated on single and multiwall carbon nanotubes (SWNTs & MWNTs) and activated carbon were synthesized, and XRD, ICP, SEM, TEM and ASAP analyses were employed to acquire the characteristics of each catalyst. Afterwards a gas flow containing 5,000 ppm of H_2S was passed over the catalyst in gas hour space velocity (GHSV) of 5,000 h^{-1}, temperature of 65 °C, steam volume percent of 20 and O_2/H_2S ratio equal to 2. The results revealed that the catalyst supported on MWNTs exhibited higher conversion amongst its counterparts. Then effects of GHSV, steam volume percent in the feed, catalyst loading and temperature were investigated on conversion of hydrogen sulfide to elemental sulfur for tungsten sulfide catalyst decorated on MWNTs.

Key words: Hydrogen Sulfide, Oxidation, Carbon Nanotubes

INTRODUCTION

Natural gas is derived from three major sources--gas wells, condensate wells, crude oil wells--and has to be refined to become utilizable in most of its applications [1]. The first and most important step is gas sweetening, which is to eliminate sour acid gases from the gas stream. There are several methods for gas sweetening, among which amine units (DEA, MEA…) are the most popular [2-7]. The separated sour gas is forwarded to a sulfur recovery unit (SRU) thereafter, in which the hydrogen sulfide is burned into elemental sulfur. A Claus sulfur recovery unit is the most common unit for conversion of H_2S into elemental sulfur in high H_2S content sour gas streams [8-10]. The Claus SRU consists of thermal and catalytic segments. In thermal segment hydrogen sulfide is combined with stoichiometric amount of air or a mixture of air/oxygen and heated to the point that a third of H_2S is combusted in a very exothermic reaction [11, 12].

$$H_2S+3/2O_2 \rightarrow SO_2+H_2O \qquad \Delta H=-4147.2\ kJ/mol \tag{1}$$

A portion of the remaining H_2S reacts with sulfur dioxide, the product of above reaction, to form elemental sulfur and steam as indicated in reaction 2 which is also exothermic.

$$2H_2S+SO_2 \leftrightarrow 3/x\ S_x^0+2H_2O \qquad \Delta H=-1165.6\ kJ/mol \tag{2}$$

The outlet stream is cooled and the elemental sulfur is condensed into liquid phase. The gas phase is directed to the catalytic segment, which is comprised of series of catalytic reactors to have the remnant of H_2S converted to elemental sulfur. The gas leaving the last reactor is directed to the tail gas treatment unit [13-15].

In Claus process normally alumina (Al_2O_3) and titania (TiO_2) are employed as supports [16]. Fe, Co and Ni are the catalytic metals which are deposited on the aforementioned supports [17,18]. Alumina is the most common support in conversion of hydrogen sulfide to sulfur. The strength lies in its potential to disperse active metal catalyst. Indeed, numerous reactions take place between alumina and metal oxide in transition state and some of the formed particles are too resistant against sulfidation, which is a defect that lowers the activity of catalyst [19,20]. H_2S oxidation is extremely exothermic and causes a major temperature escalation in catalytic bed, considering the low thermal conductivity of alumina which gives rise to the troublesome hot spots [16]. High temperature favors the reverse reaction in reaction (2) and lowers the conversion of H_2S to elemental sulfur.

Studies on oxidation of hydrogen sulfide revealed that the introduction of steam into the reactor boosts the oxidation of H_2S into elemental sulfur in temperatures between 200 °C to 300 °C and in streams having 15% v/v hydrogen sulfide. It appears the optimum temperature for catalytic reaction over alumina support is approximately 250 °C. Increasing the temperature speeds up the reverse Claus reaction and decreases the conversion of H_2S to elemental sulfur, in 300 °C the conversion is about 41% [12].

Nickel sulfide catalyst on SiC support has exhibited eminent performance in continuous and discontinuous processes. In batch process this catalyst has the capacity to convert 2,500-3,500 ppm of H_2S, and higher selectivity is observed when implementing iron oxide over SiC rather than alumina [21,22]. This is mostly pertinent to higher thermal conductivity of SiC in comparison with alumina and also to the acid sites over SiC that facilitate the production of elemental sulfur.

Activated carbon is also employed as support in this reaction [23-31]. H_2S oxidation over activated carbon loaded with sodium carbonate is investigated in streams having a concentration of 1,500-5,500 ppm of H_2S, revealing that production of elemental sulfur is highly sensitive to temperature variation and in low velocities of gas stream there is an increase in production of elemental sulfur [26].

Carbon nanotubes are deemed a great catalyst support for this reaction [32]. Oxidation of H_2S over NiS_2 nanocatalysts deposited

†To whom correspondence should be addressed.
E-mail: alizadehsa@ripi.ir

on multi wall carbon nanotubes (MWNTs) has exhibited a significant degree of ascent in conversion of this reaction [33]. Nickel sulfide catalysts have exhibited a better performance when deposited on MWNT rather than SiC support.

The first step in the present research was synthesis of single wall carbon nanotubes (SWNTs) and MWNTs. Then these nanotubes and activated carbon were loaded with tungsten sulfide particles and underwent the oxidation of H_2S. Effects of parameters like temperature, metal loading, steam ratio and GHSV on conversion of H_2S to elemental sulfur were investigated.

MATERIALS AND METHODS

1. Catalyst Preparation

MWNTs and SWNTs were obtained with chemical vapor deposition (CVD) method [34,35]. Ammonium meta-tungstate ($(NH_4)_6W_{12}O_{39}{\cdot}xH_2O$) was used to load tungsten particles on CNTs in the following way. It was dissolved in distilled water and ethanol mixture with a 1 : 1 volume ratio and the resulting solution was spilled on pure CNTs and sonicated. The solution was then dried for 2 hours in 110 °C and then the mixture was calcinated from room temperature to 500 °C with a slope of 2 °C/min in the presence of the air. To prevent the oxidation of CNTs the air inlet was interrupted at 300 °C and the catalyst was calcinated in the presence of N_2. Then the dried samples were analyzed by ICP to determine the loading of the metal on the CNTs. After calcinations in 300 °C a stream of 1%vol. H_2S and 99%vol. of helium was passed through catalyst bed to have tungsten oxide turned into tungsten sulfide.

2. Characterization Techniques

Scanning electron microscopy (SEM) images were obtained with a Philips, XL30 device. Gold was used as the conductive material for sample coating. The pore size and surface area measurements were performed with a micrometrics ASAP 2010 instrument by adsorption of nitrogen at 77 K. X-ray diffraction measurements were conducted using the standard powder diffraction procedure carried out with a Philips diffractometer (PW-1840) (Lump 3ukα, λ=1.54A°). TEM images were obtained with a Philips, CM 200 device in the Department of Material Science at Sharif University of Technology.

The sulfur content was determined with a high temperature measurement of sulfur content using IR detector and UOP 864 method with a LECO CS600 at the analysis labs of the research institute of the petroleum industry. H_2S concentration was analyzed using a Mettler potentiometer (DL 70 ES), with an accuracy of ±1% of ±1 mL equipped with an Ag-Ag_2S electrode (DM 141-SC) and UOP 163 method with detection threshold of 0.5 ppm.

3. H_2S Oxidation Setup

Selective oxidation of H_2S was carried out in an apparatus working isothermally under atmospheric pressure. A schematic flow diagram of the catalytic oxidation setup is shown in Fig. 1. The properties of the reactor and the setup system are described in detail in our previous works [36,37]. The reactor was vertically mounted in an electrical furnace; the temperature was controlled by a thermal indicator controller. The flow rates of the gases (O_2, He, H_2S) were monitored and controlled with Bronkhorst mass flowmeters linked to a JUMO (dTRON 304) electronic control units. All lines were maintained at 120 °C with electrical tracing tapes to avoid any condensation before the analysis.

The catalyst was heated from room temperature to the reaction temperature (heating rate of 5 °C min^{-1}) in the presence of He. At this point the reactant flow was added.

RESULTS AND DISCUSSION

The XRD pattern of tungsten sulfide decorated multi-wall and

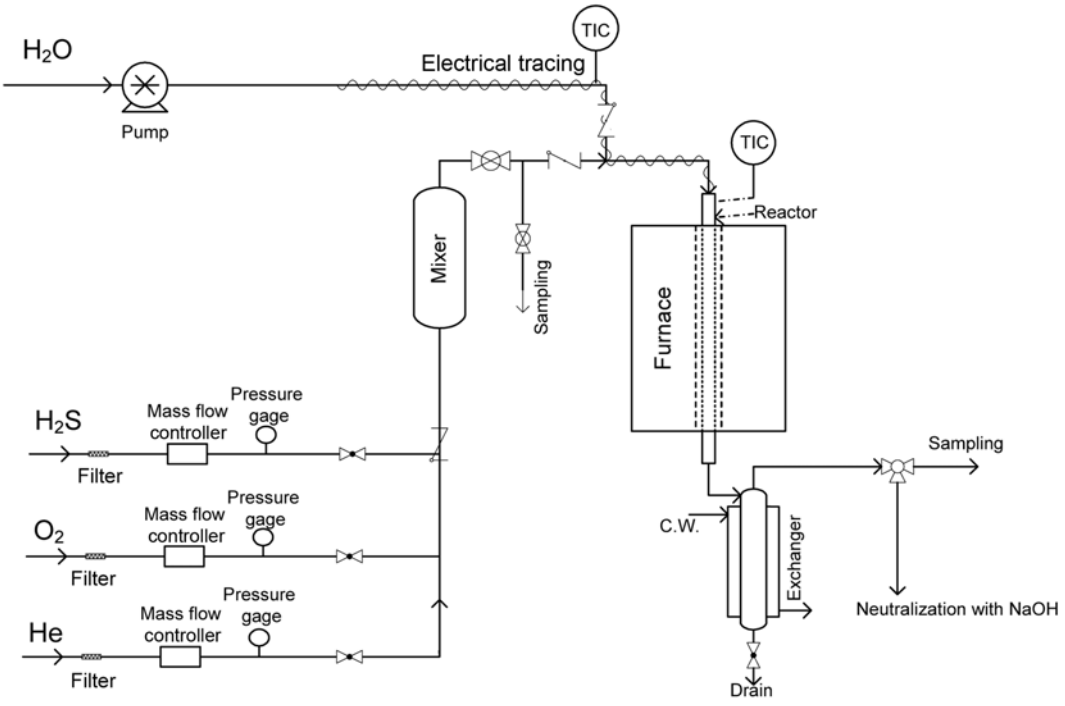

Fig. 1. Schematic flow diagram of the catalytic oxidation setup.

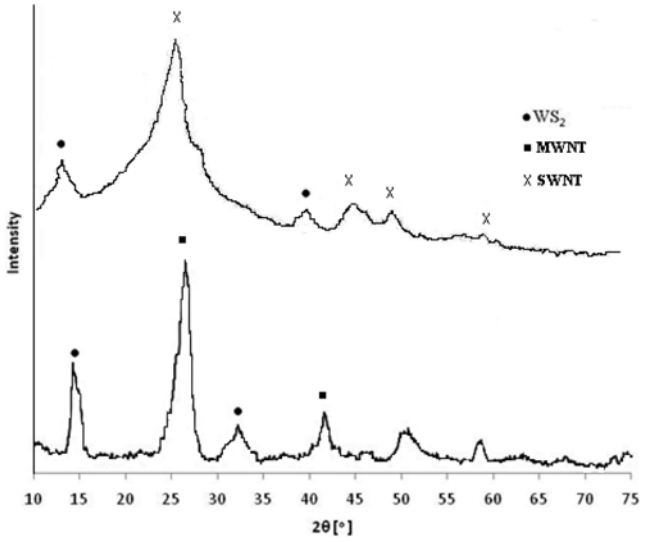

Fig. 2. XRD patterns of SWNTs and MWNTs decorated with tungsten sulfide.

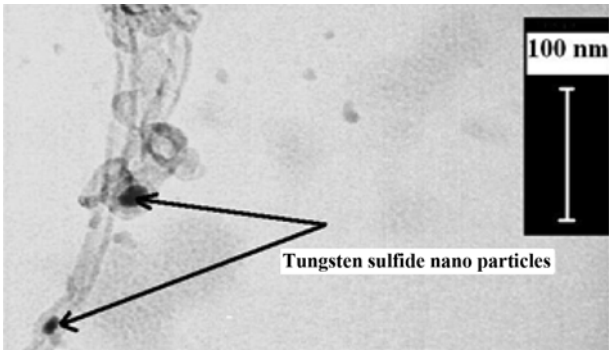

Fig. 3. TEM image of deposited tungsten sulfide particles on MWNTs.

single-wall carbon nanotubes is illustrated in Fig. 2. The peaks corresponding to MWNTs were observed in 2θ=25, 42, and those corresponding to SWNTs in 2θ=26, 43, 48 and 56. Also, peaks corresponding to tungsten sulfide were identified as is previewed in Fig. 2. TEM image in Fig. 3 corroborates the existence of metal particles on carbon nanotubes. In this image black dots represent tungsten sulfide particles deposited inside MWNTs.

1. Effect of Support Materials

The performances of the catalysts of tungsten sulfide on SWNTs, MWNTs and Norit activated carbon have been compared. All three catalysts were tested at the identical conditions (passing gas stream containing 5,000 ppm H_2S, steam volume percent of 20, ratio of oxygen to H_2S equal to 2, GHSV of 5,000 h^{-1} and temperature of

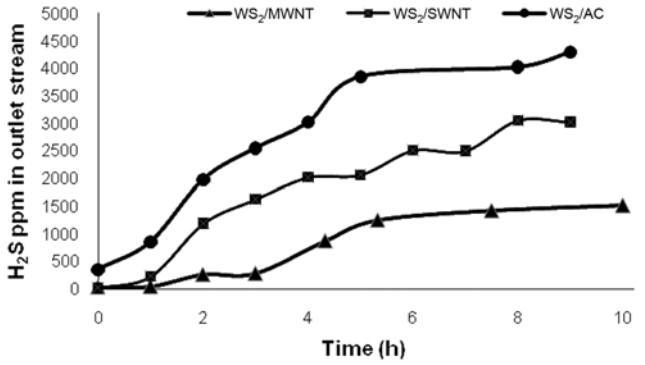

Fig. 4. Results of removal of H_2S by 5 wt% tungsten sulfide deposited on SWNTs, MWNTs and activated carbon.

65 °C); the results are illustrated in Fig. 4.

The ASAP analysis for CNTs and activated carbon presented in Table 1 reveals that the pore size of the CNTs structures lies in the mesopore area, which decreases the mass transfer resistance, whereas the pore size distribution of activated carbon is mainly in micro scale that hinders diffusion of water, H_2S (reducing agent) and O_2 (oxidizing agent) inward. Introduction of a thin layer of water on the surface of activated carbon covers up the pores, thus lessening the contact area of reacting gases and catalyst sites; this situation does not take place for CNT mesopores. According to the ICP results (Table 1), the percentage of active components in MWNTs is more than SWNTs and activated carbon, which can be related to the higher pore diameter of MWNTs.

It is obvious from the results in Table 1 that although activated carbon has a greater surface than single wall and multi wall nanotubes, but still the surface of MWNTs decreases from 110 m^2/g to 100 m^2/g (almost 10%), whereas the reduction is twice as much for activated carbon for which the surface decreases from 887 m^2/g to 707 m^2/g.

Also, regarding the confinement effect and subsequent reduction of partial pressure of reactants, the oxidation rate on CNT catalysts rises drastically, which corroborates the results of other research groups [33].

In spite of higher surface area, SWNTs exhibit a lower H_2S removal than MWNTs. Considering that water does not readily channel through SWNT [38], the formed elemental sulfur is not easily washed out, so it accumulates and blocks the catalyst sites, slowing down the conversion of H_2S. Total sulfur analysis for WS_2/SWNT and WS_2/MWNTs after approximately 10 h of reaction demonstrates the remaining sulfur in SWNT to be 7.74 wt% and in MWNTs to be 5.82 wt%, which confirms the aforementioned theory that sulfur piles up more on SWNTs surface in comparison with MWNTs.

According to the ASAP results (Table 1) average pore diameter

Table 1. ASAP and ICP analysis for tungsten sulfide deposited on activated carbon, SWNTs and MWNTs before and after reaction

Catalyst	Metal content (wt%)	Surface area (m^2/g) before test	Surface area (m^2/g) after test	Average pore diameter by (nm)	Pore volume of pores (cm^3/g)
WS_2/MWNTs	4.91	110	100	16.3	0.483
WS_2/SWNTs	4.82	303	268	10.0	0.934
WS_2/AC	4.74	887	707	2.9	1.129

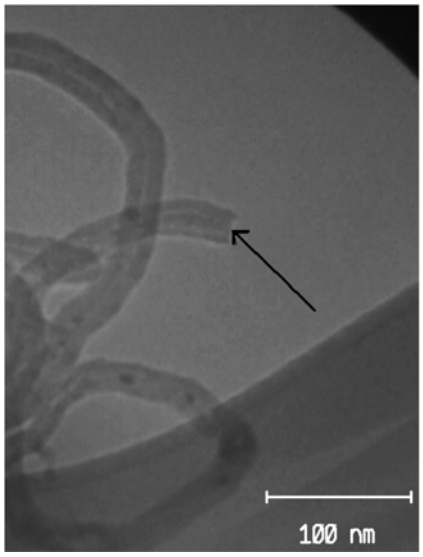

Fig. 5. TEM image of MWNTs after modification.

of SWNTs and MWNTs employed in these experiments are, respectively, 10.0 nm and 16.3 nm (Table 1), and the diameter of catalysts particles deposited on these supports is in the range of 10-20 nm (Fig. 3); therefore, it appears that most of the SWNTs pores are being obstructed by catalyst particles. The theory that states CNTs act as nanoreactors in H_2S oxidation process is more probable for MWNTs. Also, with regard to catalyst particle size, they are better dispersed in MWNTs that have a greater diameter than SWNTs. It appears that catalyst particle size has to be reduced if SWNTs are to be employed as support for catalysts so that they won't block the pores. Taking into account that MWNTs functions better than activated carbon and SWNTs, the effects of other process parameters on tungsten sulfide catalyst deposited on MWNTs were studied.

To attain better distribution of metal catalyst, initially MWNTs were dissolved in 30 vol% nitric acid solution and stirred for 16 hours, and after filtration and drying it was rinsed in 30 vol% nitric acid and this time stirred for 18 hours at 100 °C followed by filtration and drying. This procedure opens the caps at both ends of an MWNT as illustrated in Fig. 5. The ICP analysis revealed that the tungsten sulfide loading augmented from 4.91 wt% to 5.9 wt%, which means 20% increase in the amount of deposited metal. The amount of deposited metal is of outmost importance for industrial purposes. This increase is of great importance when it comes to producing a notable quantity of catalyst on industrial scale.

The ASAP results confirm a 140.2 m^2/g surface area that in comparison with former 110 m^2/g denotes that the foretold procedure is an effective step in enhancing the properties of MWNTs. Therefore, prior to deposition of tungsten sulfide catalysts, MWNTs were optimized using the aforementioned procedure.

2. Effect of Steam Ratio

Selecting MWNTs as support, the experiment was conducted at lower temperature than sulfur melting point to investigate the effect of steam ratio in inlet gas stream. Catalyst was tested at the identical conditions (passing gas stream containing 5,000 ppm H_2S, and 20 vol% steam, ratio of oxygen to H_2S equal to 2, GHSV of 5,000 h^{-1} and temperature of 65 °C). The conversion of H_2S to elemental sulfur was calculated through Eq. (3):

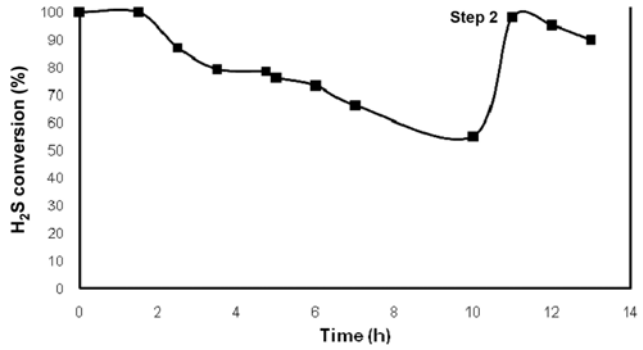

Fig. 6. Hydrogen sulfide conversion in the presence of water.

$$\text{Conversion } (\%) = \frac{[H_2S]_{in} - [H_2S]_{out}}{[H_2S]_{in}} \times 100 \quad (3)$$

where in Eq. (3), $[H_2S]_{in}$ and $[H_2S]_{out}$ are the concentration of H_2S in inlet and outlet streams in ppm, respectively. The results display 55% conversion of H_2S after 10 h of reaction. Then the H_2S flow was interrupted for about 1 h keeping a constant rate of steam flowing. H_2S injection was reinitiated after an hour maintaining 4,000 ppm of H_2S in the inlet gas stream.

As illustrated in Fig. 6, subsequent to passing steam over catalyst bed (in absence of H_2S in gas stream) the catalyst is somehow regenerated and regains its capacity in removing hydrogen sulfide.

It seems that by formation of a thin film of water on the catalyst surface, the sulfur particles are washed off and the surface is revived for further reaction. Introduction of a thin layer of water to sulfur particles increases the ionization of hydrogen sulfide particles into HS^- ions and accelerates the oxidation. A similar pattern was already observed for NiS_2 catalyst [33].

Because of the mildly low surface tension between MWNTs walls and water (72 mNm^{-1}) [33], water can readily wet the inner surface of tubes and move alongside its axis; therefore, the formed sulfur particles are slowly washed off the inside of the tubes towards the outer surface of tubes. Actually, metal deposited CNTs act as a nanoreactor in oxidation of hydrogen sulfide and cause an increase in partial pressure of gas phase reactants, raising the oxidation rate [33]. Total pressure is generally constant since steam is compressed and sulfur particles which initially reside in the gas phase are transferred to solid phase. Rate of the reaction is directly proportional to H_2S partial pressure. The sulfur particles formed on the outer surfaces of CNTs are vividly illustrated in Fig. 7.

As pictured in Fig. 7(b) the average metal particle size is 10-20 nm and mean diameter of the sulfur particles is 20-30 nm, which means they are actually in nano scale, which is of significant importance. The EDAX analysis of catalyst sample (Fig. 8) after oxidation reaction also approves the production of sulfur particles in presence of tungsten sulfide catalyst. According to the EDAX analysis the weight percent of sulfur and tungsten particles on the catalyst is 53.11% and 46.89%, respectively, which equals 1.656 mol of elemental sulfur and 0.255 mol of tungsten.

3. Effect of Metal Loading

Another parameter which might have an effect on conversion of H_2S into elemental sulfur is the metal loading on MWNTs. Three catalysts, respectively, including 5, 10 and 15 wt% of tungsten sulfide deposited on MWNTs were prepared. These catalysts were em-

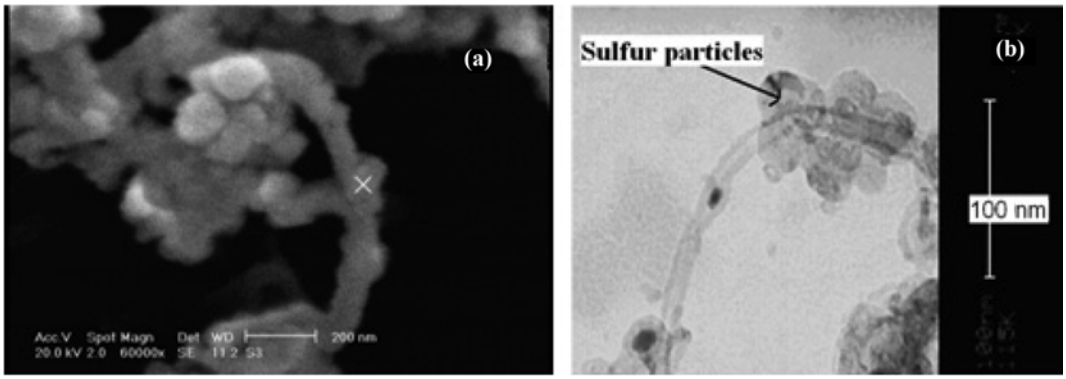

Fig. 7. (a) SEM and (b) TEM images of produced sulfur particles on outer wall of MWNTs.

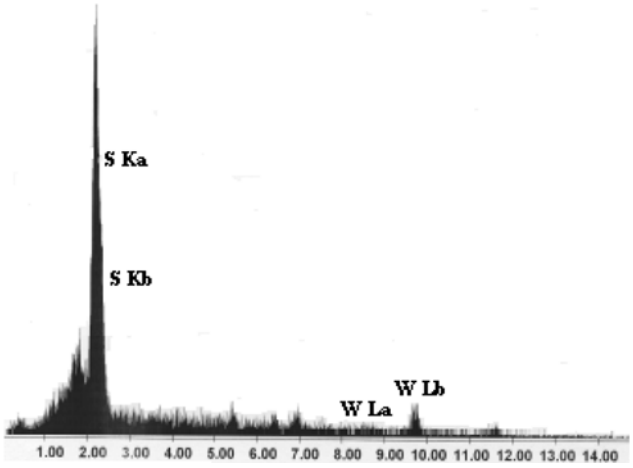

Fig. 8. EDAX analysis of catalyst sample after oxidation reaction.

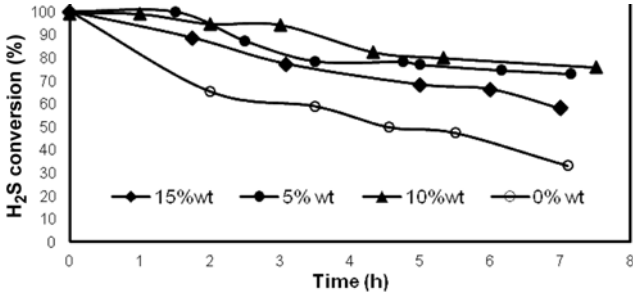

Fig. 9. Effect of catalyst loading on conversion of H_2S.

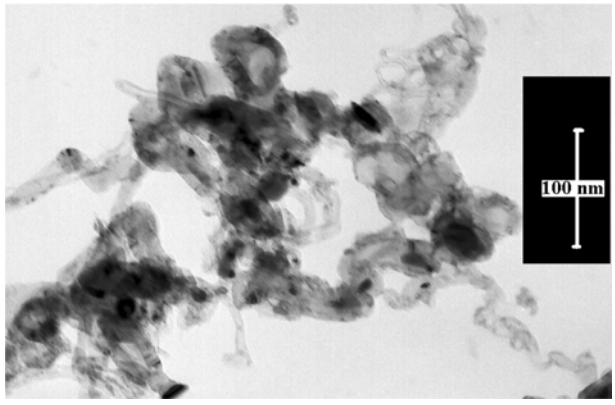

Fig. 10. TEM image of tungsten sulfide particles agglomerated on MWNTs surfaces.

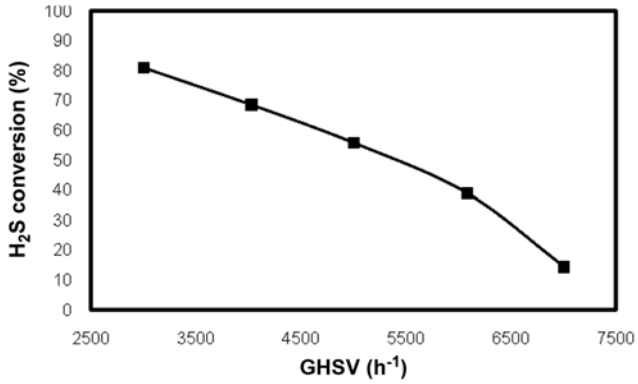

Fig. 11. Effect of GHSV on H_2S conversion into elemental sulfur.

ployed in the process of removing hydrogen sulfide from a stream containing 5,000 ppm H_2S, 20 vol% steam, O_2/H_2S=2 and balanced He. The GHSV was 5,000 h^{-1} and experiments were carried out at atmospheric pressure and 65 °C. The results are displayed in Fig. 9.

The results reveal that conversion of hydrogen sulfide and metal loading on the support are inversely proportional. With regard to the catalyst cluster size (Fig. 7), which is between 10-20 nm, it appears that by adding to the metal loading the dispersion of catalyst particles inside MWNTs abates and also the additional loading of metal, blocks some of the MWNTs pores and disturbs their role as nanoreactors. Fig. 10 is a TEM picture of MWNTs decorated with 15 wt% of tungsten sulfide catalyst, clearly showing agglomeration and aggregation of metal catalyst on some parts of MWNTs support. Dark dots are tungsten sulfide particles agglomerated on MWNTs Surfaces. To attain the maximum conversion, one has to optimize metal loading (% wt), metal cluster size, and diameter of MWNTs, which will be the scope of our future research.

4. Effect of Gas Hour Space Velocity

The effect of GHSV on the conversion of H_2S is depicted in Fig. 11 for a stream containing 5,000 ppm H_2S, 20 vol% steam, O_2/H_2S= 2 and balanced He at atmospheric pressure and 65 °C, using catalyst 5 wt% tungsten sulfide. Higher GHSV means less residence time, which generally reduces the conversion of H_2S to elemental sulfur. High GHSVs are normally the choice of industry to avoid

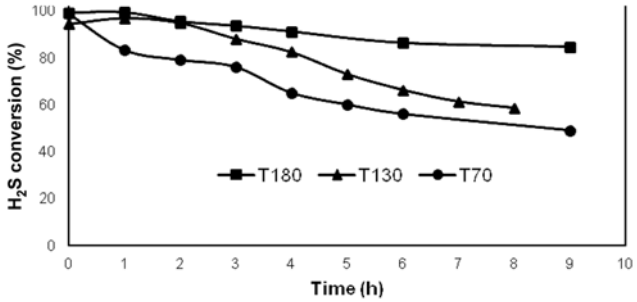

Fig. 12. Effect of temperature on H_2S conversion into elemental sulfur.

corrosion [39]. Operating at lower temperature reduces corrosion and permits lower GHSVs that will result in higher Claus efficiency. Considering that in this study the oxidation is done at a temperature lower than the melting point of sulfur, proper conversion will be reachable in low GHSV, if the catalytic beds are enlarged.

5. Effect of Temperature

Conversion of hydrogen sulfide in gas stream having 5,000 ppm of H_2S was investigated at three temperatures: 180 °C, 130 °C and 70 °C. GHSV, steam ratio and O_2/H_2S were kept same as in previous experiments. As illustrated in Fig. 12, there is a decreasing trend in conversion of H_2S and increasing in the amount of hydrogen sulfide in the outlet stream. When approaching the melting point of sulfur there is acceleration in the conversion of H_2S to elemental sulfur; also, the formed sulfur particles readily leave the surface of catalyst. Research has proved that at temperatures above the sulfur melting point (considering the exothermic Claus reaction), there is the possibility of reverse Claus reaction [16,23]. Therefore, mild temperatures lower the possibility of reverse Claus reaction and reproduction of H_2S. But since there is a flow of steam in the environment of the reaction, the sulfur particles on the surface of catalyst are washed out, leaving the catalyst active sites open to the oxidation reaction, making the conversion of H_2S possible at temperatures below the sulfur melting point.

CONCLUSION

Examining hydrogen sulfide oxidation on tungsten sulfide catalyst supported on activated carbon, SWNTs and MWNTs reveal a higher rate of conversion of hydrogen sulfide to elemental sulfur for catalysts supported on MWNTs. Studying the effect of metal loading shows that plus 10 wt% metal loading decreases the dispersion of the catalytic particles as well as blockage of carbon nanotubes pores, as a result of which the role of carbon nanotubes as nano-reactors is disrupted, which leads to a drop in conversion. Increasing GHSV results in the decrease of conversion. Considering that in this study the oxidation is done in a temperature lower than the melting point of sulfur, proper conversion is reachable in low GHSV. The regeneration of catalyst employing steam is another important fact of this research.

REFERENCES

1. Gas Processors Suppliers Association, Engineering Data Book, Vol. 2, 12th Ed. (2004).
2. R. N. Maddox, Gas and Liquid Sweetening, Campbell Petroleum Series, Oklahoma (1998).
3. H. Pahlavanzadeh and M. Farazar, *Korean J. Chem. Eng.*, **26**, 1112 (2009).
4. R. Wang, *Sep. Purif. Technol*., **31**, 111 (2003).
5. S. Mikhail, T. Zaki and L. Khalil, *Appl. Catal. A*, **227**, 265 (2002).
6. H. H. Funks, D. Fraenkel and V. H. Houlding, US Patent, 96,049 A1 (2002).
7. J. Graham and C. Yaun, US Patent, 6,858,192 B2 (2005).
8. E. Laperdrix, A. Sahibeddine, G. Costentin, M. Bensitel and J. C. Lavalley, *Appl. Catal. B*, **27**, 137 (2000).
9. W. D. Monnery, K. A. Hawboldt, A. Pollock and W. Y. Svrcek, *Chem. Eng. Sci.*, **55**, 5141, (2000).
10. J. S. Chung, S. C. Paik, H. S. Kim, D. S. Lee and I. S. Nam, *Catal. Today*, **35**, 37 (1997).
11. S. Mendioroz, V. Munoz, E. Alvarez and J. M. Palacios, *Appl. Catal., A*, **132**, 111 (1995).
12. D. Rolke, P. Cornel, R. Lell, K. Stetzer and G. Neuroth, US Patent, 5,256,384 (1993).
13. J. R. Graham and J. Cheng, US Patent, 7,241,430 B2 (2007).
14. B. Cao, S. Wang and Q. Yuan, *Chem. Eng. J.*, **118**, 133 (2006).
15. R. Miller, US Patent, 3,672,125 (1972).
16. S. W. Chun, J. Y. Jang, D. W. Park, H. C. Woo and J. S. Chung, *Appl. Catal. B*, **16**, 235 (1998).
17. S. J. Jung, M. H. Kim, J. K. Chung, M. J. Moon, J. S. Chung, D. W. Park and H. C. Woo, *Stud. Surf. Sci. Catal.*, **146**, 621 (2003).
18. K. V. Bineesh, D. K. Kim, H. J. Cho and D. W. Park, *J. Ind. Eng. Chem.*, **16**, 593 (2010).
19. E. Keller, S. Ramani, D. Allison, S. Lusk, N. Hatcher, L. Swinney, K. Kirkendall, G. Torres, P. Stewart and T. Pruitt, US Patent, 7,226,572 B1 (2007).
20. A. Carlsson and V. G. J. Heeringen, US Patent, 0,047,201 A1 (2009).
21. P. Nguyen, D. Edouard, J. M. Nhut, M. J. Ledoux, C. Pham and C. P. Huu, *Appl. Catal. B*, **76**, 300 (2007).
22. N. Keller, C. P. Huu and M. J. Ledoux, *Appl. Catal. A*, **217**, 205 (2001).
23. D. Nguyen and T. Bandosz, *Micropor. Mesopor. Mater.*, **92**, 47 (2006).
24. J. Klein and K. D. Henning, *Fuel*, **63**, 1064 (1984).
25. S. Yasyerli, G. Dogulsen and T. Doguimur, *Catal. Today*, **117**, 271 (2006).
26. S. Bashkova, F. S. Baker, X. Wu, T. R. Armstrong and V. Schwartz, *Carbon*, **45**, 1354 (2007).
27. A. Bagreev and T. J. Bandoz, *Carbon*, **39**, 2303 (2001).
28. A. Primavera, A. Trovarelli and P. Andreussi, *Appl. Catal. A*, **173**, 185 (1998).
29. A. Adib, A. Bagreev and T. J. Bandosz, *Environ. Sci. Technol*., **34**, 686 (2000).
30. T. J. Bandosz, *Carbon*, **37**, 483 (1999).
31. T. J. Bandsosz, *J. Colloid Interface Sci*., **246**, 1 (2002).
32. H. Shang, C. Liu, Y. Xu, J. Qiu and F. Wei, *J. Nat. Gas Chem*., **15**, 203 (2006).
33. J. M. Nhut, C. P. Huu, N. Keller and M. J. Ledoux, *Catal. Today*, **92**, 91 (2004).
34. A. M. Rashidi, M. M. Akbarnejad, A. A. Khodadadi, Y. Mortazavi and A. Ahmadpour, *Nanotechnol*, **18**, 315605 (2007).
35. A. Mohamadalizadeh, J. Towfighi, A. M. Rashidi, A. Mohajeri and

M. M. Golkar, *Ind. Eng. Chem. Res*., **50**, 8050 (2011).
36. A. Mohamadalizadeh, J. Towfighi, A. M. Rashidi, M. Manteghian, A. Mohajeri and R. Arasteh, *Korean J. Chem. Eng.*, **28**, 1221 (2011).
37. R. Habibi, A. Rashidi, J. Towfighi and A. Mohamadalizadeh, *Appl. Surf. Sci*., **257**, 434 (2010).
38. L. Guana, H. Lia, Z. Shi and Z. Gu, *Solid State Commun.*, **141**, 459 (2007).
39. A. Mohamadalizadeh, J. Towfighi, A. M. Rashidi, A. Mohajeri, S. Sattari and M. Manteghian, US Patent, 168,018 A1 (2011).